

## Band structure of strain-balanced GaAsBi/GaAsN superlattices on GaAs

J. Hwang and J. D. Phillips

*Department of Electrical Engineering and Computer Science, University of Michigan, Ann Arbor, Michigan 48109-2122, USA*

(Received 3 February 2011; published 31 May 2011)

GaAs alloys with dilute content of Bi and N provide a large reduction in band-gap energy with increasing alloy composition. GaAsBi/GaAsN heterojunctions have a type-II band alignment, where superlattices based on these materials offer a wide range for designing effective band-gap energy by varying superlattice period and alloy composition. The miniband structure and effective band gap for strain-balanced GaAsBi/GaAsN superlattices with effective lattice match to GaAs are calculated for alloy compositions up to 5% Bi and N using the  $\mathbf{k}\cdot\mathbf{p}$  method. The effective band gap for these superlattices is found to vary between 0.89 and 1.32 eV for period thickness ranging from 10 to 100 Å. The joint density of states and optical absorption of a 40/40 Å GaAs<sub>0.96</sub>Bi<sub>0.04</sub>/GaAs<sub>0.98</sub>N<sub>0.02</sub> superlattice are reported demonstrating a ground-state transition at 1.005 eV and first excited transition at 1.074 eV. The joint density of states is similar in magnitude to GaAs, while the optical absorption is approximately one order of magnitude lower due to the spatially indirect optical transition in the type-II structure. The GaAsBi/GaAsN system may provide a new material system with lattice match to GaAs in a spectral range of high importance for optoelectronic devices including solar cells, photodetectors, and light emitters.

DOI: [10.1103/PhysRevB.83.195327](https://doi.org/10.1103/PhysRevB.83.195327)

PACS number(s): 73.21.Cd

### I. INTRODUCTION

Semiconductor alloy compounds with large electronegativity variation, often termed highly mismatched alloys, possess dramatic changes in electronic and optical properties with only small alloy concentrations. Highly mismatched alloys of GaAsBi and GaAsN have received much attention due to their wide range of achievable band-gap energy. GaAsN with dilute nitrogen content has demonstrated materials with desired narrow band-gap properties<sup>1</sup> resulting from shifting the conduction-band edge relative to GaAs, though their use in device applications has been limited due to substantial degradation of electron mobility in the material.<sup>2</sup> GaAsBi similarly offers a means of shifting the band gap relative to GaAs,<sup>3</sup> primarily through altering the valence-band edge. Heterojunctions of GaAsN/GaAsBi are expected to have a type-II band lineup, and provide a further range of band-gap energy and a means of engineering carrier transport.<sup>4</sup> Furthermore, GaAsBi/GaAsN superlattices would offer a means for strain-balanced structures on technologically important GaAs substrates due to compressive or tensile strain for GaAsBi/GaAsN materials. The band gap versus lattice constant relationships for GaAsBi and GaAsN and schematic concept for the GaAsBi/GaAsN superlattice are shown in Fig. 1. In this work, the band structure of strain-balanced GaAsBi/GaAsN is calculated using for varying alloy composition and superlattice layer thickness to determine realistically achievable effective band-gap energies for this material system. The results of the band-structure calculations are then used to determine the near-band-edge density of states and optical-absorption coefficient.

### II. METHODS

#### A. Overview

The electronic band structure of GaAsBi/GaAsN strain-balanced superlattices with (001) crystal orientation was calculated using an eight-band  $\mathbf{k}\cdot\mathbf{p}$  method, and compared

to the self-consistent solution to the Schrodinger and Poisson equations.<sup>5</sup> Superlattice period and thickness were varied for structures that were strain-balanced with an effective lattice match to GaAs, for Bi and N content up to 5%. Details for the calculation methods and material parameters are described in the following.

#### B. Material parameters

Lattice constants and elastic constants of GaAsBi and GaAsN layer were obtained using the virtual crystal approximation with the parameters of GaAs,<sup>6</sup> GaN,<sup>6</sup> and GaBi.<sup>7</sup> Results of theoretical studies were used for GaBi, where experimental data on this material are generally lacking.<sup>7</sup> It should be noted that the alloy compositions studied in this work are well within the range of previously achieved values of 5% for GaAsN,<sup>8</sup> 10% for GaAsBi,<sup>9</sup> and agree with prior experiments that follow the band anticrossing model.<sup>10,11</sup> GaAs material with dilute concentrations of Bi results in a band-gap reduction primarily resulting from a valence-band shift, which may be explained by the valence-band anticrossing (VBAC) model.<sup>10</sup> The valence-band maximum for GaAsBi was calculated by applying the VBAC model,

$$E_V = \frac{E_{Bi} + H_{GaAs} + \sqrt{(H_{GaAs} - E_{Bi})^2 + 4C_{Bi-GaAs}^2}}{2} \quad (1)$$

with

$$H_{GaAs} = -\frac{\hbar^2}{2m_0} [(k_x^2 + k_y^2)(\gamma_1 + \gamma_2) + k_z^2(\gamma_1 - 2\gamma_2)] + \Delta E_{VBM}x, \quad (2)$$

where  $E_{Bi} = 0.4$  eV,  $C_{Bi-GaAs} = 1.55$  eV, and  $\Delta E_{VBM} = 0.8$  eV. Concurrently, the conduction-band minimum of GaAsBi layer was approximated using the virtual crystal approximation,

$$E_C = E_g(\text{GaAs}) - \Delta E_{CBM}x, \quad (3)$$

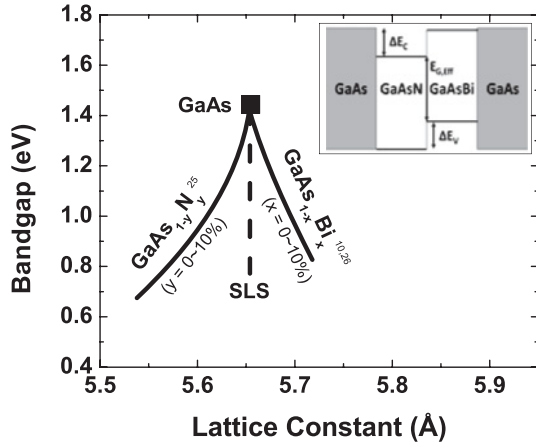


FIG. 1. Band-gap energy versus lattice constant for GaAsN<sup>25</sup> and GaAsBi<sup>10,26</sup> dilute alloys and (inset) schematic of strain-balanced GaAsBi/GaAsN superlattice with effective lattice match to GaAs.

where  $\Delta E_{CBM} = E_C(\text{GaAs}) - E_C(\text{GaBi}) = -2.1$  eV. In contrast, GaAs with dilute nitrogen concentration results in a band-gap reduction primarily resulting from a shift in the conduction-band minimum. The band-gap energy and band alignment can be similarly described by the conduction-band anticrossing (CBAC) model given by<sup>11</sup>

$$E_C = \frac{E_N + E_{C,\text{GaAs}} - \sqrt{(E_N - E_{C,\text{GaAs}})^2 + 4C_{\text{N-GaAs}}^2}}{2}, \quad (4)$$

where  $E_N = 1.65$  eV and  $C_{\text{N-GaAs}} = 2.7$  eV. The GaAsBi/GaAsN superlattice has a corresponding type-II band lineup with a potential well for electrons and holes in GaAsN and GaAsBi layers, respectively. It should be noted that GaAsN exhibits significant deviations from the BAC model due to disorder in the alloy system, where N-cluster states and related interactions between N states alter the band structure. A closer fit to experimental data is provided by the linear combination of the resonant nitrogen states (LCINS) model.<sup>12</sup> Similar behavior may also occur for GaAsBi, though the materials growth technology is still in its infancy. The BAC model was employed in this work in order to provide a more direct interpretation of trends related to the type-II superlattice band structure that are not clouded by deviations related to effects described in LCINS and similar models, or deviations related to material synthesis methods. Furthermore, the BAC model has been shown to provide excellent agreement for the band-gap energy of both GaAsN (Ref. 11) and GaAsBi (Ref. 10) relevant to the superlattice calculations presented in this work.

### C. Strain balanced criteria

Strain-balanced superlattices were investigated for structures with individual layer thickness of up to 100 Å, which is below the critical thickness predicted by the Matthews-Blakeslee model.<sup>13</sup> Alternating layers of tensile (GaAsN) and compressive (GaAsBi) strain can be used to minimize the total

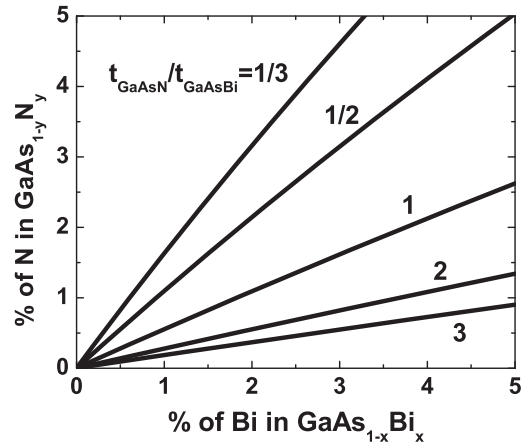


FIG. 2. Strain balanced composition of Bi and N for several thickness ratios of GaAsBi and GaAsN layers.

average strain energy of the superlattice, where the condition of zero average in plane can be achieved based on the relations<sup>14</sup>

$$t_1 A_1 \varepsilon_1 a_2 + t_2 A_2 \varepsilon_2 a_1 = 0, \quad (5)$$

$$a_0 = \frac{A_1 t_1 a_1 a_2^2 + A_2 t_2 a_2 a_1^2}{A_1 t_1 a_2^2 + A_2 t_2 a_1^2}, \quad (6)$$

$$A = C_{11} + C_{12} - \frac{2C_{12}^2}{C_{11}}, \quad (7)$$

where  $a_0$ ,  $a_1$ , and  $a_2$  represent lattice constants ( $a_1 > a_0 > a_2$ ) for the substrate with constant  $a_0$ , and  $t_1$  and  $t_2$  define the thickness of each layer. According to these relations, strain-balanced GaAsBi/GaAsN superlattices with effective lattice match to GaAs can be obtained by controlling the thickness of GaAsBi and GaAsN layers. Figure 2 shows a series of Bi and N compositions in GaAsBi and GaAsN, respectively, which satisfy the strain-balanced criteria in the superlattice for several ratios of layer thickness. In the following calculations, 4% Bi and 2.1% N are chosen under the strain-balanced condition corresponding to equivalent thickness of the GaAsBi and GaAsN layers.

### D. Band-structure calculation by the k·p method

The energy band structure and wave functions of the superlattice were calculated using eight-band  $\mathbf{k}\cdot\mathbf{p}$  perturbation theory within the envelope function approximation, which is suitable for describing the band structure near the zone center where the envelop function is slowly varying.<sup>15</sup> The  $\mathbf{k}\cdot\mathbf{p}$  methodology has been similarly applied to GaInNAs (Ref. 16) and type-II GaAsN/GaAsSb (Ref. 17) quantum wells, demonstrating good agreement with experimental measurements. In future work, the  $\mathbf{k}\cdot\mathbf{p}$  model may also be adapted to account for interactions between nitrogen (or bismuth) states based on experimental or first-principles calculations, as has been done previously for GaInAsN/GaAs quantum wells.<sup>18</sup> In this approximation, two  $8 \times 8$   $\mathbf{k}\cdot\mathbf{p}$  Hamiltonian matrices describing the band structure of the bulk constituent material satisfy the relation<sup>19</sup>

$$H^i \Psi_j(\mathbf{r}) = e_j \Psi_j(\mathbf{r}) \begin{cases} i = \text{GaAsBi, GaAsN} \\ j = \text{CB, HH, LH, SO} \end{cases} \quad (8)$$

in each layer, where terms representing energy-band offsets and hydrostatic and shear strain effects were included in the matrix elements. The wave function  $\Psi_j(\mathbf{r})$  was expanded in the basis set of the cell-periodic wave function expressed by

$$\Psi_j(\mathbf{r}) = \sum_j f_j(z) \exp(ik_x x) \exp(ik_y y) |j\rangle, \quad (9)$$

where  $f_j(z)$  is the envelope function of the  $j$ th band of the superlattice and  $|j\rangle$  is the Kane basis function of the zincblende structure satisfying the relation

$$\Psi(\mathbf{r} + \mathbf{d}) = \exp(i\mathbf{q} \cdot \mathbf{d})\Psi(\mathbf{r}), \quad (10)$$

where  $\mathbf{d}$  is the period of the superlattice and  $\mathbf{q}$  is the superlattice wave vector. In addition, the envelope function and the first derivative of  $f_j(z)$  are required to be continuous at the interface between the constituent materials of the superlattice. In this work, additional assumptions of the Hamiltonian parameters for the conduction-band Kane parameter  $F$ , Kohn-Luttinger parameters  $\gamma_1$ ,  $\gamma_2$ , and  $\gamma_3$ , and the matrix elements of the momentum operator between conduction and valence band  $\langle s|p_x|x\rangle$  were assumed to be equivalent to GaAs,<sup>6</sup> due to the lack of available data for GaAsBi and GaAsN, and the expectation that variation in these parameters would be insignificant across the range of the dilute alloy compositions studied.

The envelope function approach of the eight-band  $\mathbf{k}\cdot\mathbf{p}$  method provides a set of eight coupled second-order differential equations in the variable  $z$ , where  $k_z$  is replaced by  $-i\partial/\partial z$ . The equations were solved numerically using a transfer-matrix algorithm.<sup>19</sup> The coupled differential equations may be written as

$$\sum_{j=1}^8 \left[ A_{ij} \frac{\partial^2}{\partial z^2} - i B_{ij} \frac{\partial}{\partial z} + C_{ij} \right] f_j(z) = \varepsilon f_i(z), \quad (11)$$

$$i = 1, 2, \dots, 8$$

and modified to first-order coupled differential equations using a new  $16 \times 1$  column vector  $\Phi(z)$  given by

$$\Phi_i(z) = \begin{cases} f_i(z), & i = 1, 2, \dots, 8 \\ \sum_{j=1}^8 -A_{ij} \frac{\partial f_j}{\partial z} - i B_{ij} f_j(z), & i = 9, 10, \dots, 16 \end{cases} \quad (12)$$

satisfying the relation

$$\frac{\partial \Phi(z)}{\partial z} = \begin{pmatrix} -iA^{-1}B & -A^{-1} \\ \varepsilon - C & 0 \end{pmatrix} \Phi(z). \quad (13)$$

Because the solution of the first-order homogeneous differential equation is exponential, the solution of Eq. (13) can be described by the exponential matrix

$$\Phi(z) = \exp \left[ \begin{pmatrix} -iA^{-1}B & -A^{-1} \\ \varepsilon - C & 0 \end{pmatrix} z \right] \Phi(0), \quad (14)$$

where the solution is continuous at the interface between the layers. Energy eigenvalues  $\varepsilon$  are obtained according to the translational symmetry of the superlattice. If  $d$  is a period of the superlattice,  $\Phi(z)$  and the wave function of the superlattice should follow the relation

$$\Phi(d) = \exp(iqd)\Phi(0), \quad (15)$$

where  $q$  is the superlattice wave vector in the growth direction. The eigenvalue problem may then be described by

$$\exp \left[ \begin{pmatrix} -iA^{-1}B & -A^{-1} \\ \varepsilon - C & 0 \end{pmatrix} d \right] \Phi(0) = \exp(iqd)\Phi(0) \quad (16)$$

to calculate the energy-band structure and wave functions for the superlattice.

### E. Miniband structure with self-consistent solution of Schrödinger-Poisson equations

The spatial dependence of minibands in superlattices with finite periods was also investigated using one-dimensional calculation of the self-consistent solution of Schrödinger-Poisson equations.<sup>5,20</sup> The superlattice miniband profile was determined by this method including strain effects, where the Schrödinger equation was solved to obtain energy eigenvalues and wave functions of the superlattice based on the transfer-matrix formulation. The superlattice structure was divided by  $N$  segments, where the time-independent Schrödinger equation for the  $i$ th segment is written as<sup>21</sup>

$$\frac{d^2}{dz^2} \Psi_i(z) + \tilde{\kappa}_i^2 \Psi_i(z) = 0 \quad (z_{i-1} \leq z \leq z_i) \quad (17)$$

with the boundary conditions

$$\Psi_{i-1}(z_{i-1}) = \Psi_i(z_{i-1}), \quad (18)$$

$$\frac{1}{m_{i-1}^*} \frac{d}{dz} \Psi_{i-1}(z_{i-1}) = \frac{1}{m_i^*} \frac{d}{dz} \Psi_i(z_{i-1}), \quad (19)$$

where  $\tilde{\kappa}_i = \sqrt{2m_i^*/\hbar^2(E - V_i)}$  and  $m_i^*$  is the effective mass of charge carriers in  $i$ th layer. Considering the boundary conditions and combining all relations between two adjacent layers, the 0th and  $(N+1)$ th layer can be related as

$$\begin{pmatrix} \Psi_0(z_0) \\ \frac{1}{m_0^*} \frac{d}{dz} \Psi_0(z_0) \end{pmatrix} = \mathbf{M} \times \begin{pmatrix} \Psi_{N+1}(z_{N+1}) \\ \frac{1}{m_{N+1}^*} \frac{d}{dz} \Psi_{N+1}(z_{N+1}) \end{pmatrix}, \quad (20)$$

$$\mathbf{M} = \prod_{i=1}^N \begin{pmatrix} \cos(\tilde{\kappa}_i \cdot d_i) & -\frac{m_i^*}{\tilde{\kappa}_i} \sin(\tilde{\kappa}_i \cdot d_i) \\ \frac{\tilde{\kappa}_i}{m_i^*} \sin(\tilde{\kappa}_i \cdot d_i) & \cos(\tilde{\kappa}_i \cdot d_i) \end{pmatrix} \quad (21)$$

to determine  $\Psi$  and  $E$ . In this work, the numerical calculation of the transfer method formulation was performed using the argument principle method.<sup>21</sup>

The results from the Schrödinger equation solution can be used to calculate the carrier distribution in the superlattice and may then be incorporated in the Poisson equation,<sup>20</sup>

$$\frac{d}{dz} \left( \varepsilon_s(z) \frac{d}{dz} \right) \phi(z) = -\frac{q}{\varepsilon_0} [n(z)], \quad (22)$$

where  $\varepsilon_s(z)$  is the dielectric constant and  $\phi(z)$  is electrostatic potential distribution which satisfies the relation

$$V(z) = -q\phi(z) + \Delta E(z), \quad (23)$$

where  $\Delta E$  defines the band offset at the interfaces of the superlattice. The calculations were performed iteratively until the results of the Schrödinger and Poisson equations converged.

The electron effective mass of GaAsBi and the hole effective mass of GaAsN were assumed to be equal to GaAs

effective mass values since the conduction band and valence band are almost unchanged when a small amount of Bi and N are incorporated in GaAs, respectively.<sup>22</sup> The electron effective mass of GaAsN was obtained based on the relation<sup>11</sup>

$$m_{\text{eff}}^*(E) = m_{\text{GaAs}}^* \left\{ 1 + \frac{C_{\text{N-GaAs}}^2 x}{(E_{\text{N}} - E)^2} \right\}. \quad (24)$$

The hole effective mass of GaAsBi is not well known, where predictions have only estimated that the values would be higher than that of GaAs.<sup>3</sup> In this work, the heavy-hole and light-hole effective mass were assumed to be  $m_{\text{hh}}^* = 0.55$  and  $m_{\text{lh}}^* = 0.10$ , respectively.

### F. Absorption coefficient

The near-band edge density of states and optical-absorption coefficient were studied due to their major importance for device applications. The calculations of these parameters were all based on the results from the  $\mathbf{k}\cdot\mathbf{p}$  band-structure calculations. From the dispersion relations, constant transition energy surface in  $\mathbf{k}$  space can be obtained. By evaluating the volume between two adjacent surfaces, which represent transition energy  $E$  and  $E + dE$ , and dividing it by the volume in which each electron state occupies, the joint density of states of the superlattice was obtained. The absorption coefficient is given by<sup>23</sup>

$$\alpha(\hbar\omega) = \frac{2\pi}{\hbar} \frac{e^2}{m_0^2} \left( \frac{\hbar}{2\omega n_r c \epsilon_0} \right) \sum_{n,n'} \int d\mathbf{K} |\langle n, \mathbf{K} | p_x | n', \mathbf{K} \rangle|^2 \times \delta[E_n(\mathbf{K}) - E_{n'}(\mathbf{K}) - \hbar\omega] \quad (25)$$

neglecting the Coulomb interaction between electrons and holes, and considering only  $x$ -polarized light (normal incidence to the superlattice). The  $\delta$  function in the integration was evaluated by counting the number of states at  $\mathbf{K}$ , and the number of states was multiplied by the matrix element of momentum operator,  $\langle n, \mathbf{K} | p_x | n', \mathbf{K} \rangle$ . With the envelope function approximation of the superlattice wave function, the matrix element of the momentum operator can be written as<sup>24</sup>

$$\langle n, \mathbf{K} | p_x | n', \mathbf{K} \rangle = \sum_{j,j'} \langle j, n | p_x | j', n' \rangle \int_0^d f_{j,n}^*(\mathbf{K}, z) f_{j',n'}(\mathbf{K}, z) dz, \quad (26)$$

where the  $p_x$  is the momentum operator  $-i\hbar \frac{\partial}{\partial x}$ , and  $f_{j,n}(z)$  represents the envelope function of the  $j$ th basis of the  $n$ th band. For the term  $\langle j, n | p_x | j', n' \rangle$ , only the  $\langle x | p_x | s \rangle$  term is a nonzero, and was assumed to be equivalent to GaAs for the small composition of Bi and N in this work. The value of the matrix element for the momentum operator was obtained from

$$E_p = \frac{2}{m_0} |\langle x | p_x | s \rangle|^2, \quad (27)$$

where  $E_p$  for GaAs was assumed to be 28.8 eV from Ref. 6.

## III. RESULTS AND DISCUSSION

### A. Band structure

A representative band structure for a GaAs<sub>0.96</sub>Bi<sub>0.04</sub>/GaAs<sub>0.979</sub>N<sub>0.021</sub> superlattice with 80-Å period thickness cal-

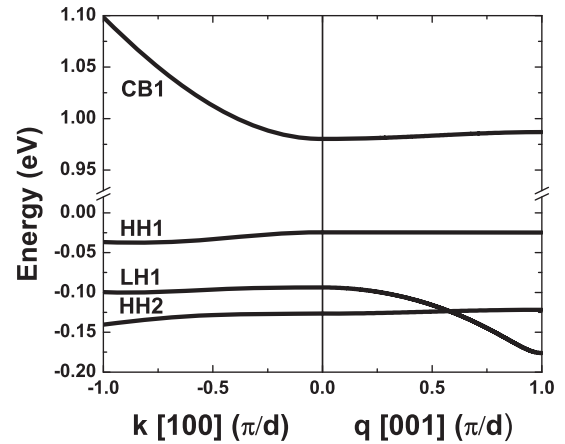


FIG. 3. Miniband structure of 40-Å/40-Å GaAs<sub>0.96</sub>Bi<sub>0.04</sub>/GaAs<sub>0.979</sub>N<sub>0.021</sub> superlattice with effective band-gap energy of 1 eV.

culated by the  $\mathbf{k}\cdot\mathbf{p}$  method is shown in Fig. 3. The conduction band contains one confined miniband (CB1) and a continuum of states at the edge of the conduction-band offset. The valence band contains confined minibands corresponding to the first heavy hole (HH1), the first light hole (LH1), and the second heavy hole (HH2). The effective band-gap energy for this superlattice, defined as the energy separation between lowest energy states in the conduction and valence bands (CB1-HH1), shows a value of 1 eV. It should be noted that this effective band-gap energy has not been previously achieved for a lattice matched III-V system to GaAs. While strained quantum well and quantum dot systems have succeeded in achieving such narrow band-gap materials on GaAs, they do not offer a means for achieving sufficiently thick active layers that are required for devices such as solar cells and photodetectors. The energy-momentum relations are shown for both the in-plane directions and the direction normal to the superlattice. For the in-plane direction, the band structure is isotropic for  $k_x$  and  $k_y$ , while the curvature differs dramatically for the direction normal to the superlattice. The range of effective band-gap energies achievable for the GaAsBi/GaAsN superlattice were investigated by varying the alloy composition up to 5% and superlattice period up to 100 Å with equivalent thickness for the GaAsBi and GaAsN layers. The variation in effective band gap spans from 0.89 to 1.32 eV in this range, as shown in Fig. 4. The superlattice band structure was found to be primarily dependent on the superlattice period, strain parameters, and band-gap energy and band offsets of the materials. These parameters have a high degree of certainty for these calculations.

Uncertain parameters for the  $\mathbf{k}\cdot\mathbf{p}$  calculations include the matrix element of the momentum operator  $E_p$  and Kohn-Luttinger parameters  $\gamma_1$ ,  $\gamma_2$ , and  $\gamma_3$ , which may be significantly altered in GaAsN and GaAsBi dilute alloys. Calculations were performed with large variations in these parameters to determine their influence on the calculated band structure and effective band gap. Varying parameters  $E_p$  (for GaAsN, conduction-band states)  $\gamma_1$ ,  $\gamma_2$ , and  $\gamma_3$  (for GaAsBi, valence-band states) by up to a factor of 2 for the GaAs<sub>0.96</sub>Bi<sub>0.04</sub>/GaAs<sub>0.979</sub>N<sub>0.021</sub> superlattice results in a similar result, with a deviation of <5% for the effective band

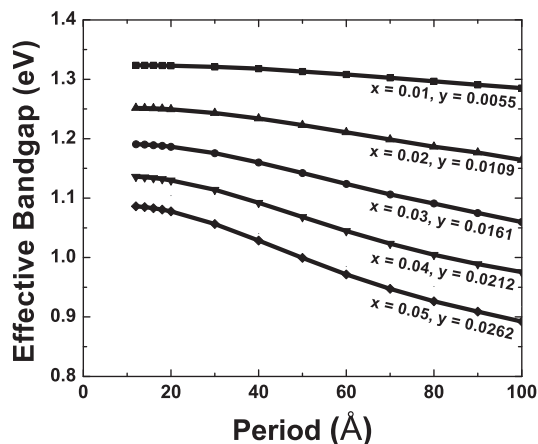


FIG. 4. Effective band-gap energy for GaAsBi/GaAsN superlattices with matched layer thickness, varying period thickness, and variable alloy composition.

gap. The small deviation suggests a relatively low sensitivity of the results presented to the chosen  $\mathbf{k}\cdot\mathbf{p}$  parameters.

**B. Effective mass**

The electron and hole effective masses in the superlattice growth direction can be calculated for these structures assuming parabolic relationships near the band edge according to the relation

$$\frac{1}{m^*} = \frac{1}{\hbar^2} \frac{d^2\varepsilon}{dk^2}. \tag{28}$$

The effective mass of electrons and holes increases as the superlattice period increases, as shown in Fig. 5. This increase is consistent with a decrease in tunneling probability with increasing layer thickness. This trend is more pronounced in the valence band for the range of composition and period examined, with an increasing dependence on period for larger Bi/N alloy compositions. The effective mass for the conduction band demonstrates a crossover point at a period of approximately 60 Å, reflecting the

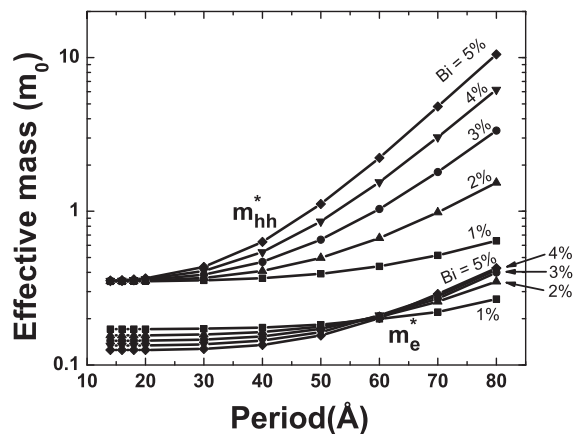


FIG. 5. Effective masses of ground-state minibands ( $m_e^*$  for CB1 and  $m_{hh}^*$  for HH1) for GaAsBi/GaAsN superlattices with matched layer thickness, varying period thickness, and variable alloy composition.

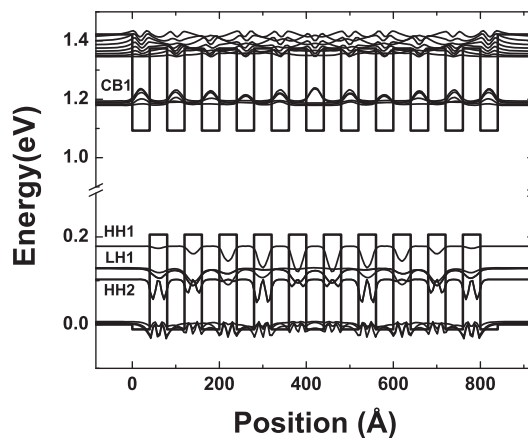


FIG. 6. Miniband structure for ten period 40-Å/40-Å GaAs<sub>0.96</sub>Bi<sub>0.04</sub>/GaAs<sub>0.979</sub>N<sub>0.02</sub> superlattice using self-consistent Schrödinger-Poisson calculations.

transition from smaller effective mass dominated by GaAsN behavior at small period thickness to larger effective mass dominated by decreased tunneling probability at large period thickness.

**C. Spatial distribution of wave functions**

Varying finite total thickness of the superlattices was investigated between 5 and 15 periods using the Schrödinger-Poisson self-consistent solution in order to evaluate the influence of finite structures and number of periods on effective band gap. The spatial distribution of wave functions for a ten period (80-Å period) GaAs<sub>0.096</sub>Bi<sub>0.04</sub>/GaAs<sub>0.979</sub>N<sub>0.021</sub> superlattice with GaAs layers at both ends is shown in Fig. 6. The effective band-gap energy of the superlattice is 1 eV, with four confined states in the bound-state region (CB1, HH1, LH1, and HH2). The conduction and the first heavy-hole band levels are in agreement with the results of the  $\mathbf{k}\cdot\mathbf{p}$  calculations, while the first light-hole and the second heavy-hole band levels differ by approximately 30 meV. The discrepancy for the position of the first light-hole and the second heavy-hole states is attributed to assumed values for the hole effective mass in GaAsBi required to evaluate the Schrödinger equation using the transfer-matrix formalism, while these values are not required for the  $\mathbf{k}\cdot\mathbf{p}$  calculations. Although the hole effective mass of GaAsBi is expected to be larger than the hole effective mass of GaAs, the value is still unknown due to lack of theoretical and experimental data. In this work, the hole effective mass of GaAsBi was used as a fitting parameter to match the transition energy for effective band-gap energy obtained by  $\mathbf{k}\cdot\mathbf{p}$ , resulting in values of  $0.55m_0$  and  $0.10m_0$  for heavy-hole and light-hole mass, respectively. In addition, the effective band-gap energy is found to match the  $\mathbf{k}\cdot\mathbf{p}$  prediction of 1.000 eV, with a variation of approximately 1.001 to 1.004 eV varying between 5 and 15 periods.

The spatial dependence of the wave functions is also examined using results of the  $\mathbf{k}\cdot\mathbf{p}$  method due to the importance of optical properties. The square of the envelope function of the superlattice at  $k_x = k_y = q = 0$  is shown as a function of the superlattice normal direction in Fig. 7. The  $s$  component of the conduction-band and  $x$  component of the valence-band

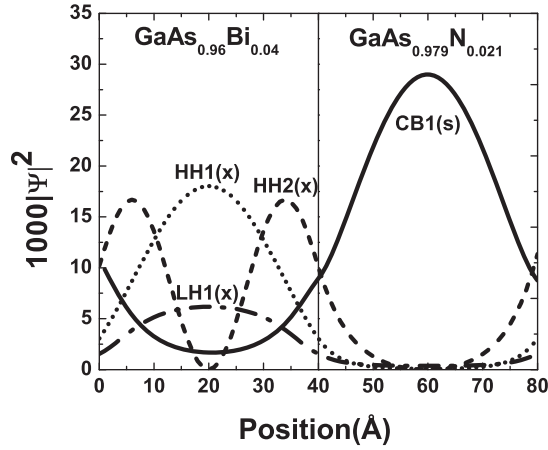


FIG. 7. Squared envelope function of the 40-Å/40-Å GaAs<sub>0.96</sub>Bi<sub>0.04</sub>/GaAs<sub>0.979</sub>N<sub>0.021</sub> superlattice. Characters *s* and *x* in the figure represent the symmetry character of the envelope function.

envelope functions are shown, corresponding to the primary components that are coupled with optical radiation at normal incidence to the superlattice. The *s* and *x* designation indicate the component of the zinc-blende zone-center cell-periodic basis function. The electrons and holes are primarily confined in the GaAsN and GaAsBi layers, respectively, with significant overlap near the GaAsBi/GaAsN interfaces.

**D. Optical properties**

The joint density of states for the superlattice including the transitions from HH1 to CB1 and LH1 to CB1 is shown in Fig. 8 for a GaAs<sub>0.96</sub>Bi<sub>0.04</sub>/GaAs<sub>0.979</sub>N<sub>0.021</sub> superlattice with 80-Å period thickness. The curve has a steplike shape due to the quantum confinement in the superlattice, with a smooth transition in the vicinity of the effective band gap due to the miniband dispersion. The joint density of states for the LH1 to CB1 transition results in a shallower transition due to the large curvature of the LH1 band in the out-of-plane direction. The optical-absorption coefficient of the superlattice for *x*-polarized light incident in the growth direction is shown in Fig. 9, assuming a full valence band and empty conduction

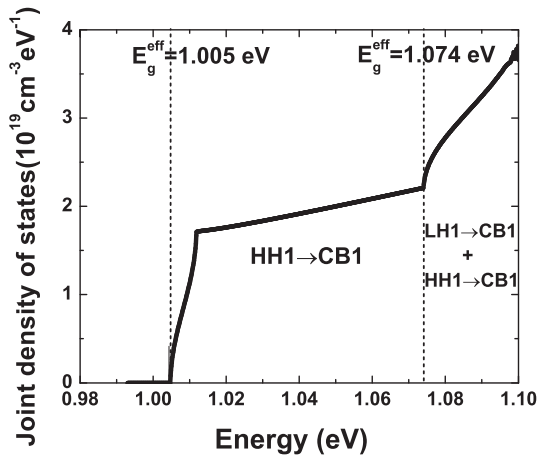


FIG. 8. Joint density of states of a 40-Å/40-Å GaAs<sub>0.96</sub>Bi<sub>0.04</sub>/GaAs<sub>0.979</sub>N<sub>0.021</sub> superlattice.

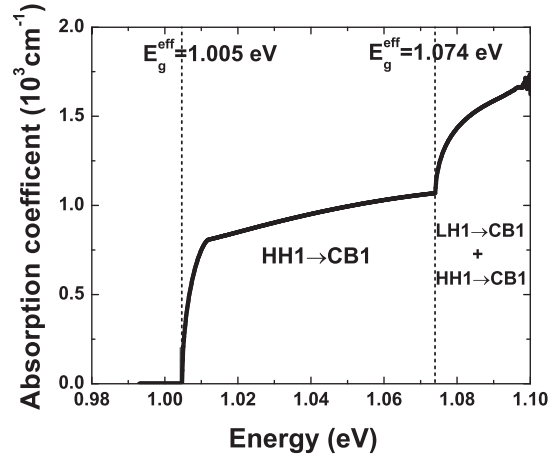


FIG. 9. Absorption coefficient of a 40-Å/40-Å GaAs<sub>0.96</sub>Bi<sub>0.04</sub>/GaAs<sub>0.979</sub>N<sub>0.021</sub> superlattice.

band. The absorption spectrum follows the steplike shape of the joint density of states, altered by the oscillator strength of the optical transition in this type-II structure. In these calculations, the Coulomb interaction between electrons and holes was not considered, which would otherwise result in excitonic peaks below the effective band-gap energy. The magnitude of the optical-absorption coefficient is approximately one order of magnitude smaller than bulk GaAs due to the spatially indirect transition, with approximately the same magnitude for joint density of states.

**IV. CONCLUSIONS**

In conclusion, the miniband structure for strain-balanced GaAsBi/GaAsN with effective lattice match to GaAs was calculated, demonstrating a range of effective band gap of 0.89–1.32 eV for Bi,N composition of less than 5% and period thickness of up to 100 Å. The energy-momentum dispersion relations show a general trend of increasing carrier effective mass with increasing period due to reduced tunneling probability, and a compositional dependence that contains a crossover point for electron effective mass due to competing mechanisms of the superlattice period and host material properties. The calculated miniband structure by the *k*·*p* method is consistent with the Schrodinger-Poisson technique, where further efforts to determine carrier effective mass are required in order to provide improved accuracy and agreement for excited-state transitions. The GaAsBi/GaAsN superlattices have a joint density of states similar to GaAs and an optical-absorption coefficient that is approximately one order of magnitude lower than GaAs due to the spatial separation of electron and hole wave functions in the type-II structure. This superlattice structure may provide a narrow band-gap material system that is lattice-matched to GaAs with optical response suitable for optoelectronic devices requiring optically thick active regions, such as a spectral band in a multijunction solar cell. Further theoretical and experimental work is desired to realize these materials and to determine optical transitions and charge-transport properties.

## ACKNOWLEDGMENTS

The authors would like to thank Jasprit Singh for discussions on the  $\mathbf{k}\cdot\mathbf{p}$  simulations, Junseok Heo for discussions on numerical methods, and Carl Fischer at MIT Lincoln Laboratory for assistance with the Schrödinger-Poisson calculations.

This work was supported as part of the Center for Solar and Thermal Energy Conversion, an Energy Frontier Research Center funded by the US Department of Energy, Office of Science, Office of Basic Energy Sciences under Award No. DE-SC0000957. J.H. gratefully acknowledges scholarship support from the STX Foundation.

- 
- <sup>1</sup>W. G. Bi and C. W. Tu, *Appl. Phys. Lett.* **70**, 1608 (1997).  
<sup>2</sup>S. Fahy, A. Lindsay, H. Ouerdane, and E. P. O'Reilly, *Phys. Rev. B* **74**, 035203 (2006).  
<sup>3</sup>T. Tiedje, E. C. Young, and A. Mascarenhas, *Int. J. Nanotech.* **5**, 963 (2008).  
<sup>4</sup>A. Sibille, in *Semiconductor Superlattices: Growth and Electronic Properties*, edited by H. T. Grahn (World Scientific, River Edge, NJ, 1995).  
<sup>5</sup>C. H. Fischer, Ph.D. thesis, University of Michigan, Ann Arbor, 2004.  
<sup>6</sup>I. Vurgaftman, J. R. Meyer, and L. R. Ram-Mohan, *J. Appl. Phys.* **89**, 5815 (2001).  
<sup>7</sup>M. Ferhat and A. Zaoui, *Phys. Rev. B* **73**, 115107 (2006).  
<sup>8</sup>S. Ikuo *et al.*, *Semicond. Sci. Technol.* **17**, 755 (2002); I. J. W. Ager and W. Walukiewicz, *ibid.* **17**, 741 (2002).  
<sup>9</sup>X. Lu, D. A. Beaton, R. B. Lewis, T. Tiedje, and M. B. Whitwick, *Appl. Phys. Lett.* **92**, 192110 (2008).  
<sup>10</sup>K. Alberi, J. Wu, W. Walukiewicz, K. M. Yu, O. D. Dubon, S. P. Watkins, C. X. Wang, X. Liu, Y. J. Cho, and J. Furdyna, *Phys. Rev. B* **75**, 045203 (2007).  
<sup>11</sup>W. Shan, W. Walukiewicz, K. M. Yu, J. W. Ager III, E. E. Haller, J. F. Geisz, D. J. Friedman, J. M. Olson, S. R. Kurtz, H. P. Xin, and C. W. Tu, *Phys. Status Solidi* **223**, 75 (2001).  
<sup>12</sup>A. Lindsay and E. P. O'Reilly, *Phys. Rev. Lett.* **93**, 196402 (2004); G. Pettinari, F. Masia, A. Polimeni, M. Felici, A. Fropa, M. Capizzi, A. Lindsay, E. P. O'Reilly, P. J. Klar, W. Stolz, G. Bais, M. Piccin, S. Rubini, F. Martelli, and A. Franciosi, *Phys. Rev. B* **74**, 245202 (2006); T. Dannecker, Y. Jin, H. Cheng, C. F. Gorman, J. Buckeridge, C. Uher, S. Fahy, C. Kurdak, and R. S. Goldman, *ibid.* **82**, 125203 (2010).  
<sup>13</sup>J. W. Matthews and A. E. Blakeslee, *J. Cryst. Growth* **27**, 118 (1974).  
<sup>14</sup>N. J. Ekins-Daukes, K. Kawaguchi, and J. Zhang, *Cryst. Growth Design* **2**, 287 (2002).  
<sup>15</sup>D. L. Smith and C. Mailhot, *Rev. Mod. Phys.* **62**, 173 (1990); M. E. Flatt, P. M. Young, L.-H. Peng, and H. Ehrenreich, *Phys. Rev. B* **53**, 1963 (1996).  
<sup>16</sup>R. J. Potter, D. Alexandropoulos, A. Erol, S. Mazzucato, N. Balkan, M. J. Adams, X. Marie, H. Carrère, E. Bedel, G. Lacoste, A. Arnoult, and C. Fontaine, *Physica E* **17**, 240 (2003).  
<sup>17</sup>A. A. Khandekar, B. E. Hawkins, T. F. Kuech, J. Y. Yeh, L. J. Mawst, J. R. Meyer, I. Vurgaftman, and N. Tansu, *J. Appl. Phys.* **98**, 123525 (2005).  
<sup>18</sup>S. A. Choulis, T. J. C. Hosea, S. Tomić, M. Kamal-Saadi, B. A. Weinstein, E. P. O'Reilly, A. R. Adams, and P. J. Klar, *Phys. Status Solidi B* **235**, 384 (2003).  
<sup>19</sup>L. R. Ram-Mohan, K. H. Yoo, and R. L. Aggarwal, *Phys. Rev. B* **38**, 6151 (1988).  
<sup>20</sup>I.-H. Tan, G. L. Snider, L. D. Chang, and E. L. Hu, *J. Appl. Phys.* **68**, 4071 (1990).  
<sup>21</sup>E. Anemogiannis, E. N. Glytsis, and T. K. Gaylord, *IEEE J. Quantum Electron.* **29**, 2731 (1993).  
<sup>22</sup>R. N. Kini, L. Bhusal, A. J. Ptak, R. France, and A. Mascarenhas, *J. Appl. Phys.* **106**, 043705 (2009); H. Suzuki, T. Hashiguchi, N. Kojima, Y. Ohshita, and M. Yamaguchi, *Presented at the Photovoltaic Specialists Conference (PVSC)*, 2009 34th IEEE, (2009) (unpublished).  
<sup>23</sup>N. F. Johnson, H. Ehrenreich, P. M. Hui, and P. M. Young, *Phys. Rev. B* **41**, 3655 (1990).  
<sup>24</sup>B. Jogai and D. N. Talwar, *Phys. Rev. B* **54**, 14524 (1996).  
<sup>25</sup>K. Uesugi, N. Morooka, and I. Suemune, *Appl. Phys. Lett.* **74**, 1254 (1999).  
<sup>26</sup>Y. Takehara, M. Yoshimoto, W. Huang, J. Saraie, K. Oe, A. Chayahara, and Y. Horino, *Jpn. J. Appl. Phys.* **45**, 67 (2006).